PHYSICAL REVIEW D **90,** 013011 (2014)

Searching for a nondiagonal mass varying mechanism in the $\nu_\mu - \nu_\tau$ system

D. R. Gratieri[1,2,*] and O. L. G. Peres[2,3,†]

[1]*Instituto de Física e Matemática, Universidade Federal de Pelotas, Caixa Postal 354, CEP 96010-900 Pelotas, Rio Grande do Sul, Brazil*

[2]*Instituto de Física Gleb Wataghin—UNICAMP, 13083-859 Campinas, São Paulo, Brazil*

[3]*Abdus Salam International Centre for Theoretical Physics, ICTP, I-34010 Trieste, Italy*

(Received 2 June 2014; published 14 July 2014)

We use atmospheric neutrino data and MINOS data to constrain the MaVaN (mass varying neutrinos) mechanism. The MaVaN model was largely studied in cosmology scenarios and comes from the coupling of the neutrinos with a neutral scalar depending on the local matter density. For atmospheric neutrinos, this new interaction affects the neutrino propagation inside the Earth, and as consequence, induces modifications in their oscillation pattern. To perform such test for a nonstandard oscillation mechanism with a nondiagonal neutrino coupling in the mass basis, we analyze the angular distribution of atmospheric neutrino events as seen by the Super-Kamiokande experiment for the events in the sub-GeV and multi-GeV range and muon neutrinos (antineutrinos) in the MINOS experiment. From the combined analysis of these two sets of data we obtain the best fit for $\Delta m^2_{32} = 2.45 \times 10^{-3}$ eV^2, $\sin^2(\theta_{23}) = 0.42$ and MaVaN parameter $\alpha_{32} = 0.28$ with modest improvement, $\Delta\chi^2 = 1.8$, over the standard oscillation scenario. The combination of MINOS data and Super-Kamiokande data prefers small values of MaVaN parameter $\alpha_{32} < 0.31$ at 90% C. L.

DOI: 10.1103/PhysRevD.90.013011 PACS numbers: 14.60.St, 14.60.Pq, 95.85.Ry

I. INTRODUCTION

Due to the observations of cosmic microwave background radiation [1,2], large scale structure [3], and Ia Supernovae [4–6], we know that the Universe is actually in accelerated expansion. A direct way to incorporate this accelerated expansion of universe into Einstein General Relativity Theory [7] is to include the cosmological constant Λ. The inclusion of this constant has the same effect of a nonzero vacuum energy density, $\rho_{\rm vac}$, in such way that the pressure $p_{\rm vac}$ and the density $\rho_{\rm vac}$ are related by a state equation with the form $p_{\rm vac} = -\rho_{\rm vac}$.

On the other hand, the accelerated expansion of the Universe can also be described by adding to the Universe content a homogeneous fluid with energy density ρ_λ, the so-called dark energy [8]. This fluid has positive energy density $\rho_{\rm DE}$, and negative pressure $p_{\rm DE}$, in such way that $p_{\rm DE} < -\rho_{\rm DE}/3$. This pressure is then responsible for the accelerated expansion of the Universe. It is a remarkable fact that 73% of the Universe's content must be in the dark energy form. Also, dark energy would be uniformly distributed in all space, and so, its density is constant in all points and times. This is in contrast with the time evolution of baryonic matter density $\rho_{\rm BM}$, that diminishes due to the expansion of the Universe. It is called the "cosmic coincidence" to the fact that today, the baryonic matter density, $\rho_{\rm BM}$ has approximately the same value of dark energy density $\rho_{\rm DE}$ [9]. To compare different cosmological models, it is common to define the density parameter Ω that it is the ratio between the density ρ with the critical density $\rho_{\rm c}$ of the Friedmann universe, $\Omega = \rho/\rho_{\rm c}$. In this sense the cosmic coincidence implies in the equality $\Omega_\Lambda = \Omega_{\rm BM}$. This coincidence can be viewed as an indicative of the existence of some dynamical effect that relates both scales of baryonic matter and of the dark energy density.

Nevertheless, among all the models in the literature that are devoted to explain the accelerated expansion of the Universe, there is a class of dynamical models that obtain the desired negative pressure due to the inclusion of a scalar field that is the responsible for the variations in the expected value of vacuum energy. As the neutrino squared mass difference, $\Delta m^2_{32} \equiv m^2_3 - m^2_2 = 2.5 \times 10^{-3}$ eV^2, where m_3 and m_2 are the masses of third and first neutrino mass state, is of same order of dark energy scale, it is straightforward to think a model in which the scalar field couple to neutrinos and hence, the total energy of the fluid can vary slowly as the neutrino density decreases [10]. In the mass varying neutrino models the inclusion of a scalar field allow the coupling of neutrino and dark energy densities due to the nonstandard neutrino-scalar coupling. The main consequence of this coupling to the neutrino physics is the fact that now the neutrino masses depends on the medium density. This field could couples neutrinos to the baryonic matter and also to the neutrino background [11]. The consequences in cosmology of MaVaN have been studied in recent years ([10–15] and references therein).

For the neutrino phenomenology the consequences of MaVaN were studied for the solar and atmospheric neutrinos [16–23]. We will use the data from Super-Kamiokande

*gratieri@ifi.unicamp.br
†orlando@ifi.unicamp.br

(SK for now) experiment [23]. In the experiment SK, down-going neutrinos, the ones that are produce in the atmosphere immediately over Super-Kamiokande detector, reaches SK with the cosine of zenith angle $\cos\theta_z \to 1$ and travels approximately 20 km in the atmosphere. On the other hand, up-going neutrinos are produced in the opposite side of the planet and cross all the Earth before reaching SK in the cosine of the zenith angle $\cos\theta_z \to -1$ direction. The so-called "up-down" asymmetry of neutrino events in SK is recognized as the first experimental corroboration of neutrino flavor oscillations. We explicit here that atmospheric neutrinos that arrives at SK from different directions travels different distances and crosses regions of very distinct densities (see next section for details). This fact makes the angular distribution of events in SK a good place to looking for dependence of medium density effects in the propagation of neutrinos. In fact, the SK experiment reported no improvement of data fit due to the inclusion of the diagonal MaVaN mechanism in the propagation of atmospheric neutrinos [23]. For our knowledge there is no analysis made for the non-diagonal MaVaN mechanism for atmospheric neutrinos.

We also apply the MaVaN model to describe the beam muon neutrinos and antineutrinos at MINOS experiment [24], where a muon neutrino or muon antineutrino beam with energy between few hundred of MeV and few GeV. The neutrino or antineutrino beam travels a few hundred of kilometers inside Earth's crust before reach the far detector. By the comparison between the number of neutrino events in near and far detector MINOS collaboration has measure precisely the standard neutrino parameters Δm^2_{32} and $\sin^2(2\theta_{23})$. See for example [24,25] and references therein. In the MaVaN context, the main difference between MINOS beam and SK is that in the former neutrinos cross only the upper crust of Earth, that can be described by a constant matter density and the latter cross a different nonconstant densities. In this way the MaVaN's effective oscillation for MINOS, with a constant density and with SK with a variable density, allows us to test the essential characteristic of the MaVaN mechanism, the density dependence of the neutrino mass differences.

The paper is organized as follows. In Sec. II we describe the framework of MaVaN that we adopt, and in Sec. II A we show the changes in neutrino oscillations due to MaVaN. Then in Sec. III we compare our results for the angular distribution of events in SK for neutrino oscillations without and with MaVaN. Also in Sec. IV we show how the MaVaN mechanism affects the allowed range of oscillation parameters for the MINOS experiment and in Sec. V we perform the χ^2 analysis of SK atmospheric neutrino combined with MINOS beam data and the constraints to the MaVaN model that we obtain. Conclusions are in Sec. VI.

II. FRAMEWORK OF MAVAN MODEL

In the neutrino mass-mixing formalism, the time evolution of neutrino flavor eigenstates is given in terms of neutrino mixing, in which one has to describe the flavor eigenstate; hence, the time evolution of atmospheric neutrinos, in the two neutrino flavor approximation, is given by the evolution equation

$$i\frac{d}{dt}\begin{pmatrix}\nu_\mu\\ \nu_\tau\end{pmatrix} = [UH_{\rm mass}U^\dagger]\begin{pmatrix}\nu_\mu\\ \nu_\tau\end{pmatrix}, \tag{1}$$

and the Hamiltonian assumes the form, in the mass basis,

$$H_{\rm mass} = \frac{\Delta m^2_{32}}{2E_\nu}\begin{bmatrix}0 & 0\\ 0 & 1\end{bmatrix}. \tag{2}$$

Here E_ν is the neutrino energy, $\Delta m^2_{32} \equiv m^2_3 - m^2_2$ is the square difference of mass eigenstates, and U is the mixing matrix,

$$U = \begin{pmatrix}c_{23} & s_{23}\\ -s_{23} & c_{23}\end{pmatrix}, \tag{3}$$

where $c_{23} = \cos\theta_{23}$, $s_{23} = \sin\theta_{23}$. The muon neutrino survival probability is

$$P(\nu_\mu \to \nu_\mu) = 1 - \sin^2 2\theta_{23}\sin^2\left(\frac{\Delta m^2_{32}L}{4E_\nu}\right), \tag{4}$$

where $\Delta m^2_{32} \equiv m^2_3 - m^2_2$ is the squared mass difference, L is the distance, and E_ν is the neutrino energy. The formalism that we adopt to include MaVaN in the neutrino propagation has the Standard Model of particles plus a light scalar field (ϕ) with mass m_S that couples with neutrinos ν_i, $i = 1, 2, 3$ and with fermion fields $f = e, n, p$. In such a model, the modification due to MaVaN is the introduction of a fermion density-dependent term in each one of the matrix elements in the neutrino mass matrix, Eq. (2). Thus, including MaVaN, the flavor neutrino evolution is described by the generalization of Eq. (1). Explicitly we have

$$i\frac{d}{dt}\begin{bmatrix}\nu_\mu\\ \nu_\tau\end{bmatrix} = H^{\rm flavor}_{\rm MaVaN}\begin{bmatrix}\nu_\mu\\ \nu_\tau\end{bmatrix}, \tag{5}$$

where the modified Hamiltonian in the MaVaN framework [26] is

$$H^{\rm flavor}_{\rm MaVaN} = UH^{\rm mass}_{\rm MaVaN}U^\dagger, \tag{6}$$

where the mixing matrix U is defined in Eq. (3) and the MaVaN Hamiltonian has the form

$$H^{\rm mass}_{\rm MaVaN} = \frac{\Delta m^2_{32}}{2E_\nu}\begin{bmatrix}\alpha^2_2 g(\rho) & \alpha^2_{32} g(\rho)\\ \alpha^2_{32} g(\rho) & 1 + \alpha^2_3 g(\rho)\end{bmatrix}. \tag{7}$$

Here α_2, α_3, and α_{32} are the MaVaN parameters and $g(\rho)$ is the function of the Earth matter density ρ that neutrinos feel while crossing the Earth. When $\alpha_2 = \alpha_3 = \alpha_{32} = 0$ we

recover the standard neutrino evolution given in Eq. (1). We can classify the behavior of the MaVaN mechanism given in Eq. (7) into two types: (a) when $\alpha_2, \alpha_3 \neq 0$ and $\alpha_{32} = 0$ and (b) when $\alpha_2 = \alpha_3 = 0$ and $\alpha_{32} \neq 0$. In the former case the neutrino survival probability, for constant density, is given by

$$P(\nu_\mu \to \nu_\mu) = 1 - \sin^2 2\theta_{23} \sin^2\left(\frac{(\Delta m^2)'_{\rm eff} L}{4E_\nu}\right), \quad (8)$$

where the effective mass scale is given by $(\Delta m^2)'_{\rm eff} \equiv \Delta m^2_{32}[1 + (\alpha_3^2 - \alpha_2^2) g(\rho)]$. In this case, when $\alpha_{32} = 0$ the amplitude of oscillations, $\sin^2 2\theta_{23}$, is the same as in the standard neutrino oscillations in Eq. (4), and the phase of the oscillations, proportional to $(\Delta m^2)'_{\rm eff}$, has now a matter density dependence. This was the case most studied in the literature [16–23]. The latter case, the Hamiltonian in the mass basis, is nondiagonal, and to our knowledge it was not explored in the literature for atmospheric neutrino phenomenology. The probability, for constant density ρ can be written as

$$P(\nu_\mu \to \nu_\mu) = 1 - \sin^2 2\theta_{\rm MaVaN} \sin^2\left(\frac{\Delta m^2_{\rm MaVaN} L}{4E_\nu}\right), \quad (9)$$

where the amplitude, $\sin^2 2\theta_{\rm MaVaN}$, and the phase of oscillations, $\Delta m^2_{\rm MaVaN}$, are different from the usual standard oscillation scenario. The MaVaN mass difference is given by

$$\Delta m^2_{\rm MaVaN} \equiv \Delta m^2_{32} \sqrt{\{2\alpha_{32}^2 g(\rho)\}^2 + 1}, \quad (10)$$

where the MaVaN mass difference depends on the medium density and the explicit expression for the amplitude is

$$\begin{aligned} \sin^2 2\theta_{\rm MaVaN} &\equiv \sin^2(2\theta + 2\eta) \\ &= [\sin(2\theta)\cos(2\eta) + \sin(2\eta)\cos(2\theta)]^2, \end{aligned} \quad (11)$$

which also has a dependence on the medium density. The angle η is defined as

$$\sin^2(2\eta) = \frac{[2\alpha_{32}^2 g(\rho)]^2}{1 + [2\alpha_{32}^2 g(\rho)]^2} \quad (12)$$

in the MaVaN case, where $\alpha_{32}^2 \neq 0$ induces that the mass basis is not diagonal and the parameter η is the mixing angle that diagonalizes the mass basis, as shown in Ref. [27]. This ensures that the nondiagonal MaVaN would induce neutrino oscillations even if the vacuum mixing angle were zero, $\theta \to 0$.

In the case of standard oscillations, see Eq. (4), we have the symmetry $\sin^2\theta_{23} \leftrightarrow \cos^2\theta_{23}$, but in the MaVaN case with $\alpha_{32}^2 \neq 0$ we have broken this symmetry, and Eq. (11) has different results for $\sin^2\theta_{23} > \cos^2\theta_{23}$ compared with $\sin^2\theta_{23} < \cos^2\theta_{23}$. For vanishing MaVaN parameters, $\alpha_{32}^2 = 0$, we have $\sin^2 2\eta \to 0$ $\eta \to 0$, and we recover the standard neutrino oscillation. For very large values of MaVaN parameters, we have $\sin^2 2\eta \to 1$, which implies that $\sin^2 2\theta_{\rm MaVaN} \to \cos^2 2\theta_{23}$. If we have large mixing angles $\theta_{23} \sim \pi/4$, we will have suppression of the amplitude, but for smaller mixing angles we will have an enhancement of the amplitude.

Most of the previous analysis of MaVaN works for the first two generations [16–21], and then their constraints are related to parameters of the first generation α_1, α_2, and α_{12}, similar to the parameters defined in Eq. (7). From Ref. [18] that provides an upper bound for the elements of matrix $|H_{12}|_{\rm MaVaN}$, $|H_1|_{\rm MaVaN} < 10^{-4}$ eV at 90% C.L. The only case that works in the MaVaN scenario for the second and third families are the Refs. [22,23]. In this paper they assume the nonzero parameters α_2 and the medium matter dependence is given by $g(\rho) = (\rho/\rho_0)^n$, where ρ is the matter density, $\rho_0 = 1$ g/cm^3, and n is a free parameter. The diagonal MaVaNs was ruled out as the dominant oscillation scenario for atmospheric neutrinos, and they constrain the n parameter to be in the range $-0.15 < n < 0.1$ at 90% C.L. [22,23].

A. Oscillation probabilities without MaVaN and with MaVaN

Now we are going to compare the oscillation probabilities without MaVaN and with MaVaN to understand the changes in the oscillation probabilities.

Most of previous analysis use a model for the MaVaN mass M_i given as a function of parameter with dimensions of energy such as $M_i = \mu_i g(\rho)$, with the index i denoting the diagonal mass eigenstates $i = 1, 2$ and the nondiagonal mass eigenstates $i = 3$; with different functions $g(\rho)$ as function of the matter density ρ, and a parameter μ_i with dimension of energy. We decide to adopt dimensionless parameters in this work, the α_i as described in Eq. (7), but we can relate our parameters α_i with the previous analysis by the replacing of $\mu_i \to \alpha_i \Delta m^2$, where Δm^2 is the relevant mass difference of the analysis.

In this paper we study the case for the nondiagonal MaVaN parameter, $\alpha_2 = \alpha_3 = 0$ and $\alpha_{32} \neq 0$ [Eq. (7)]. As an example we will use the MaVaN density dependence as used in Ref. [19,21], given by

$$g(\rho) = \tanh^2\left(\frac{\rho}{\rho_{\rm core}}\right). \quad (13)$$

We will use the matter profile of Earth that we take from [28], where ρ is the matter density that neutrino crosses, and $\rho_{\rm core} = 11.5$ g/cm^3 is the matter density at Earth core. This choice is made to generate a soft and well-behaved function even with the abrupt variations of the Earth density profile. Other choices made the computation numerically unstable

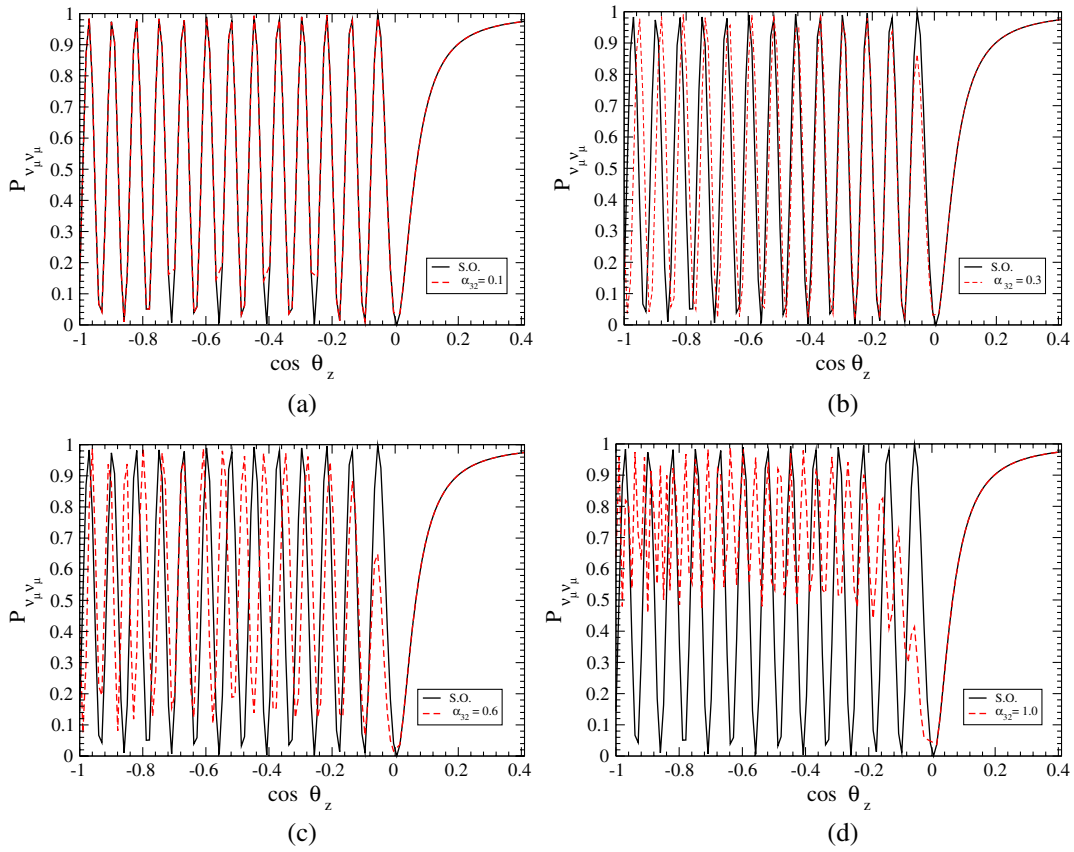

FIG. 1 (color online). Muon neutrino survival probability as a function of $\cos\theta_z$. The standard oscillation (S.O.) are shown in black solid curve and the MaVaN oscillation curves are in dashed color with the values of α_{32} indicated in each panel. In this plot we assume the values of $\sin^2(2\theta_{23}) = 1.0$ and $\Delta m^2_{32} = 2.6 \times 10^{-3}$ eV^2 and $E_\nu = 1.0$ GeV in all plots.

as reported in Ref. [22]. Also it has a finite limit for $\rho \to \infty$ and $g(\rho) < 1$ always.

We solve numerically the muon neutrino survival probability, $P(\nu_\mu \to \nu_\mu)$, for the general case of a neutrino crossing the Earth from different chords. We can relate the traveled distance by neutrino L to the zenith angle θ_z by $L = -R_{\rm E}\cos(\theta_z) + \sqrt{R^2_{\rm E}\cos^2(\theta_z) + h^2 + 2R_{\rm E}h}$, where $R_{\rm E} = 6371$ km is the Earth's radius and h is the point of the atmosphere where neutrinos are produced, approximately 20 km. For $\cos\theta_z \to 1(-1)$ we have the maximum (minimum) distance. We show in Fig. 1 the muon neutrino probability as a function of the cosine of zenith angle, $\cos\theta_z$, for fixed values of the amplitude of the mixing angle, $\sin^2(\theta_{23}) = 1/2$, for the mass difference $\Delta m^2_{32} = 2.6 \times 10^{-3}$ eV^2 and for a fixed energy $E_\nu = 1.0$ GeV and several values of α_{32}: $\alpha_{32} = 0.1$, 0.3, 0.6, 1.0. We have, respectively, the MaVaN probabilities as dashed curves and without MaVaN as solid curves in Figs. 1(a), 1(b), 1(c), and 1(d). For values of $\cos(\theta_z) > 0$, the neutrino traveled in vacuum only and the oscillation probabilities with and without MaVaN are the same. For $\cos(\theta_z) < 0$, the neutrino cross inside the Earth and the MaVaN effect begins to pop up. To see more clearly the effect of the MaVaN parameters, we can compare Fig. 1(a) that has $\alpha_{32} = 0.1$ with Fig. 1(d) that has $\alpha_{32} = 1.0$. When we increase the MaVaN parameter α_{32} for maximal mixing, the MaVaN amplitude get smaller and the oscillation phase increases, giving more fast wiggles that appear in the probability. The increase of wiggles makes the maximums and minimums move to smaller values of $\cos\theta_z$.

B. Oscillograms

The concept of oscillograms is an interesting tool to understand the complete behavior of neutrino probability in some model for neutrino oscillation. We plot in Fig. 2 the oscillograms of muon neutrino survival probability, denoted by $P_{\nu_\mu\nu_\mu}$, as a function of neutrino energy E and the cosine of zenith angle, $\cos(\theta_z)$. In Fig. 2(a), we show the standard neutrino case, and in the other plots, increasing bigger values of the MaVaN parameter. For the cosine of zenith angle, $\cos(\theta_z) > 0$, when the neutrino did not cross the Earth, we have zero MaVaN effect and for $\cos(\theta_z) < 0$, the muon survival probability is modified due to the MaVaN mechanism. For comparison we show in the upper left panel, the upper right panel, the lower left panel, and the lower right panel of Fig. 2 the MaVaN

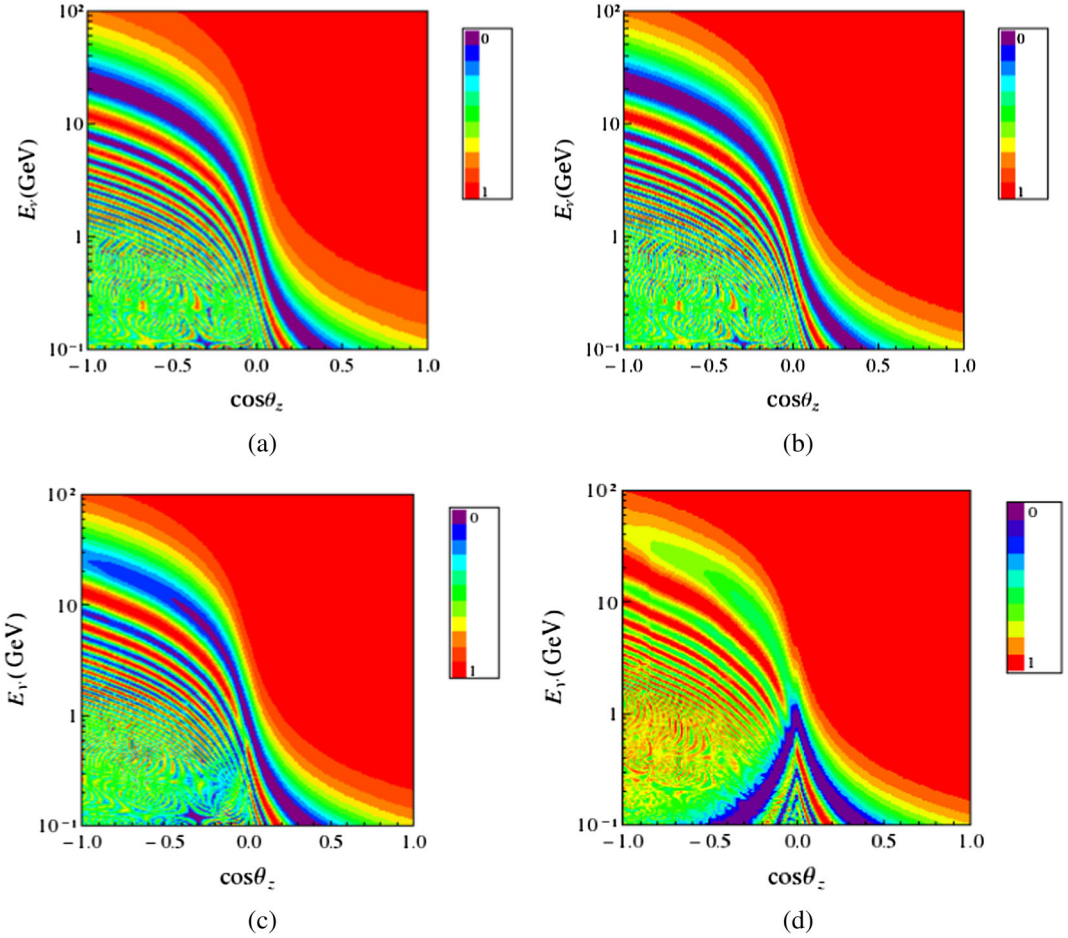

FIG. 2 (color online). In sequence—upper left, upper right, lower left, and lower right—we show the oscillogram in the plane cosine of neutrino zenith ($\cos\theta_z$) angle and neutrino energy (E_ν), for the survival probability $P(\nu_\mu \to \nu_\mu)$, respectively, for $\alpha_{32} = 0.0, 0.1, 0.5, 1.0$. We assume $\Delta m^2_{32} = 2.6 \times 10^{-3}$ eV^2 and maximal mixing angle $\sin^2(\theta_{23}) = 1/2$.

parameters α_{32}, respectively, equal to 0.0, 0.1, 0.5, and 1.0. An enhancement of $\Delta m^2_{\mathrm{MaVaN}} > \Delta m^2_{32}$ also implies that the positions of maximums and minimums is dislocated to higher values of neutrino energy. As an example of this let we look to the first minimum in $P_{\nu_\mu\nu_\mu}$ for $\cos\theta_z = 1.0$. In the former three panels of Fig. 2(a) we see that the first minimum ocurs for $E_\nu \approx 25$ GeV. In the lower-left panel, where $\alpha_{32} = 1.0$ this minimum in $P_{\nu_\mu\nu_\mu}$ had its intensity reduced (due to the increase of $\sin^2\theta_{\mathrm{MaVaN}}$) but also we see that the minimum was dislocated to $E_\nu \approx 40$ GeV. At $E_\nu \approx 25$ GeV now we see the first maximum of oscillation that for S.O. occur at $E_\nu \approx 4.5$ GeV. The same kind of displacement is found for all the maximums and minimums in the lower-left panel of Fig. 2(a) when compared with the cases in which $\alpha_{32} < 1.0$.

III. NUMBER OF MUONS AND ELECTRONS IN SUPER-KAMIOKANDE EXPERIMENT

Atmospheric neutrinos, composed muon neutrinos, and electron neutrinos are produced all around the Earth's atmosphere and travel to Super-Kamiokande from all directions. Once in the detector they interact, producing muons and electrons, and Super-Kamiokande measures the zenith angle dependence of these muons and electrons. The rate for these events can be computed as

$$N(\mu) = TN_t \int_{E_0^\nu}^{E_f^\nu} dE_\nu \int_0^1 dx \int_{-1}^1 d(\cos\theta_z) \int_0^{2\pi} d\phi_z \int_{\cos\theta_{\mu_0}}^{\cos\theta_{\mu_f}} d\cos\theta_\mu \times \left\{ \frac{d^3\Phi_{\nu_\mu}(E_\nu,\theta_z,\phi_z)}{dE_\nu d(\cos\theta) d\phi_z} \times P(\nu_\mu \to \nu_\mu) \times \frac{d\sigma_{\nu_\mu}(E_\nu,E_\mu)}{dE_\mu} \right.$$
$$\left. + \frac{d^3\Phi_{\bar\nu_\mu}(E_\nu,\theta_z,\phi_z)}{dE_\nu d(\cos\theta) d\phi_z} \times P(\bar\nu_\mu \to \bar\nu_\mu) \times \frac{d\sigma_{\bar\nu_\mu}(E_\nu,E_\mu)}{dE_\mu} \right\} \times \Theta[E_\mu(\cos\theta_z, E_\nu, \cos\theta_\mu) - E_\mu^{\min}]$$
$$\times \Theta[E_\mu^{\max} - E_\mu(\cos\theta_z, E_\nu, \cos\theta_\mu)], \tag{14}$$

where N_t is the number of targets in SK, T is the live time, E_ν is the neutrino energy, $\cos\theta_z$ is the cosine of zenith angle (θ_z) of the neutrino, ϕ_z is the azimuth angle of the neutrino, $\cos\theta_\mu$ is the cosine of zenith angle of the muon, Φ_{ν_μ} is the muon neutrino flux, $P(\nu_\mu \to \nu_\mu)$ is the muon neutrino survival probability, and $\sigma_{\nu_\mu}(E_\nu, E_\mu)$ is the differential charged current muon-neutrino cross section. For the integration boundaries, E_0^ν and E_f^ν the initial and final neutrino energies; $\cos\theta_{\mu_0}$ and $\cos\theta_{\mu_f}$ the bin of zenith angle distribution of Super-Kamiokande experiment, in this we use 10 equal bins of muon zenith angle between $\cos\theta_\mu = -1$, 1. We compute this expression for the two different types of events in SK experiment: the so-called sub-GeV data set and multi-GeV data set. They correspond, respectively, to the intervals of $(E_\mu^{\min}, E_\mu^{\max}) = (0.2, 1.2\ \text{GeV})$ and $(E_\mu^{\min}, E_\mu^{\max}) = (10.0, 100.0\ \text{GeV})$. We use the kinematics of reaction [29], defined by θ_z, θ_μ and E_ν variables to set up the allowed range of muon energy, given by the function $E_\mu(\cos\theta_z, E, \cos\theta_\mu)$, and we constrain to be in the sub-GeV and multi-GeV energy range. Notice that the zenith angle of leptons it is a function of the zenith angle of neutrinos, the scattering angle, and the energy of neutrinos, and this produces a stronger averaging effect on the original neutrino direction. For the electronlike zenith distribution of events in SK we can write

$$N(e) = TN_t \int_{E_0^\nu}^{E_f^\nu} dE_\nu \int_0^1 dx \int_{-1}^1 d\cos(\theta_z) \int_0^{2\pi} d\phi_\nu \int_{\cos\theta_{e_0}}^{\cos\theta_{e_f}} d\cos\theta_e \times \left\{ \Phi_{\nu_e}(E_\nu, \theta_\nu, \phi_\nu) \times \frac{d\sigma_{\nu_e}(E_\nu, E_\mu)}{dE_\nu dE_e} + \Phi_{\bar{\nu}_e}(E_\nu, \theta_\nu, \phi_\nu) \times \frac{d\sigma_{\bar{\nu}_e}(E_\nu, E_e)}{dE_\nu dE_\mu} \right\} \times \Theta[E_e(\cos\theta_z, E_\nu, \cos\theta_e) - E_e^{\min}]\, \Theta\,[E_e^{\max} - E_e(\cos\theta_z, E_\nu, \cos\theta_e)], \quad (15)$$

which is very similar to the muon events, with the exception that the electron neutrino did not oscillate, due to our initial assumption that we only have oscillations between muon and tau neutrinos. The muon and electron neutrino fluxes are taken from [31]. The differential cross section follows [32], where we divide the cross section into three parts, first the quasielastic neutrino scattering with finite mass corrections [33], second, the one pion contribution, and third, the DIS contribution [34]. Since the Super-Kamiokande did not discriminate between particles and antiparticles, we sum over neutrino and antineutrino types.

The muon and electron rate for atmospheric neutrinos has the uncertainties from the prediction of the atmospheric neutrino fluxes, Φ_{ν_μ} and Φ_{ν_e}, the computation that can be $\Delta(\Phi_{\nu_\mu})$, $\Delta(\Phi_{\nu_e}) = 30\%$, and the relative error $\delta(\Phi_{\nu_\mu}/\Phi_{\nu_e})$ of 5% [32]. Because of this error in the absolute normalization, we will use as the physical observable the zenith distribution of the number of events, and the absolute value of our prediction will be scaled with the experimental data. Also the smallness of the relative error of muon and electron neutrino fluxes compared with the error in the absolute number implies a stronger correlation between the fluxes of muon and electron neutrinos, which we should take into account.

We use this formalism to describe two energy ranges of SK data, the so-called sub-GeV and multi-GeV data sets for electrons and muons, Eq. (14) and Eq. (15). We compute the muon neutrino survival probability, given in Eq. (4), with the oscillation parameters given by $\Delta m_{32}^2 = 2.6 \times 10^{-3}\ \text{eV}^2$ and the amplitude $\sin^2(\theta_{23}) = 0.5$ shown as the black curve in Figs. 3(a) and 3(b), respectively, for the sub-GeV and multi-GeV samples. For these parameters we have no oscillation for $\cos\theta_z > -0.1$ and average out oscillation for $\cos\theta_z < -0.6$. Our results match the theoretical curves for the number of events for no-oscillation and standard oscillation of the SK experiment. For our computation with MaVaN probability, we use the numerical solution of Eq. (5) using the matter profile given in Eq. (13) and we compute the rate for electron and muon [given by Eq. (14) and Eq. (15)]. The result is the dashed curve in Figs. 3(a) and 3(b). The effect of nonzero MaVaN, using the same oscillation parameters and the MaVaN parameter $\alpha_{32} = 0.6$, is to distort the muon distribution making a small oscillation for cosine of lepton zenith $\cos\theta_z > 0$, coming from neutrino zenith angle $\cos\theta_\nu < 0$, due to the averaging effect mentioned after Eq. (14). Suppressing the averaging of neutrino oscillations for $\cos\theta_z < -0.6$, both behaviors are disfavored by the SK data, and from this we expect to have a constraint in the MaVaN parameter from this data.

In atmospheric neutrinos, neutrinos can come from different directions, and they probe different medium densities making the mass difference $\Delta m^2_{\text{MaVaN}}$ different at each point of the travel. On the other hand, for MINOS, the neutrino travel only crosses the upper crust, and we can assume that density along this short chord is constant. We will assume $\rho_{\text{crust}} = 3.59\ \text{g/cm}^3$ from the PREM model. We can use the results of Sec. II of the MaVaN mechanism for constant medium density, where the muon survival probability is given by Eq. (9) with the MaVaN mass difference given by Eq. (10) and the amplitude by Eq. (11). It is interesting that the functional form of the MaVaN oscillation probability is exactly like the standard oscillation probability, with the replacement $\Delta m_{32}^2 \to \Delta m^2_{\text{MaVaN}}$ and $\sin^2 2\theta_{23} \to \sin^2 2\theta_{\text{MaVaN}}$.

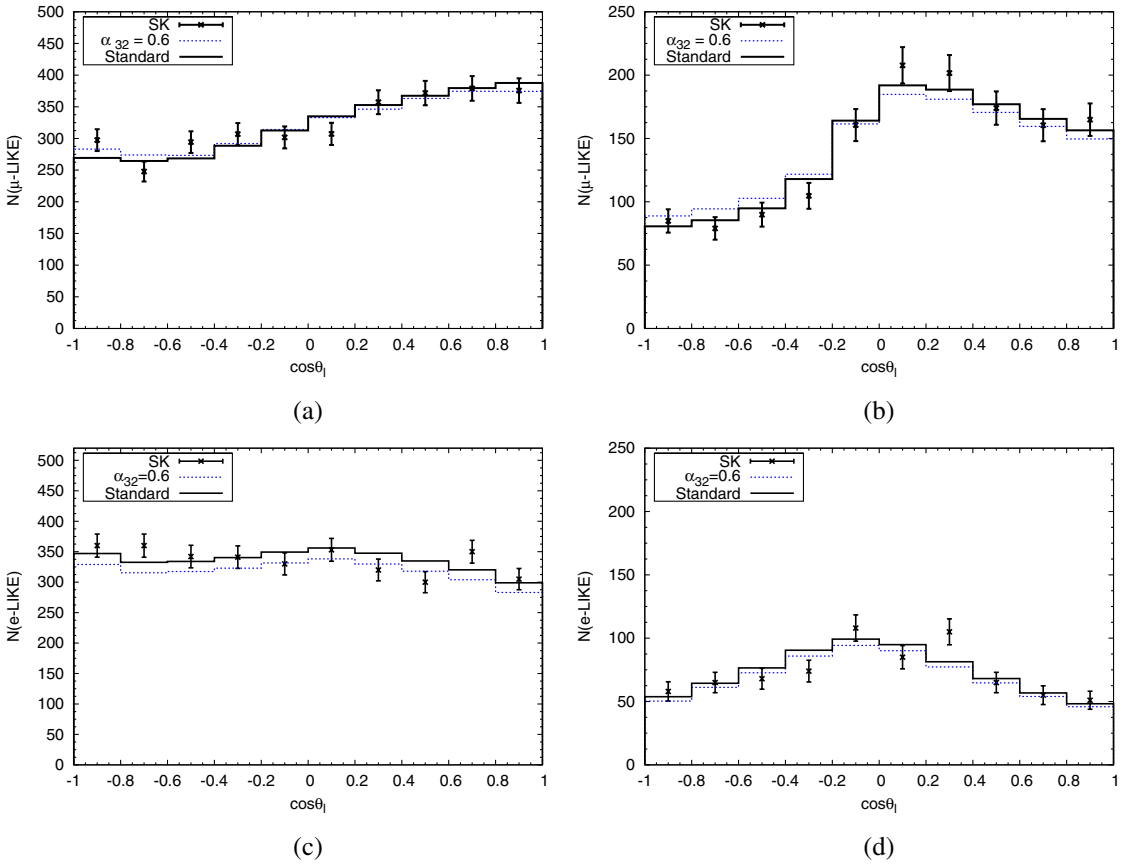

FIG. 3 (color online). In sequence, upper (bottom) panels we show the zenith distributions of muonlike (electronlike) events in SK (points). The left (right) panel are for sub-GeV (multi-GeV) energy region. Solid line refers to our calculation for the expect number of events for the case of standard neutrino oscillations ($\alpha_{32} = 0$). The dashed line refers to the case of $\alpha_{32} = 0.6$. Points refers to SK data from [35]. We assume $\Delta m^2_{32} = 2.6 \times 10^{-3}$ eV^2 and maximal mixing angle $\sin^2(\theta_{23}) = 1/2$.

IV. OFF-DIAGONAL MAVAN-INDUCED OSCILLATIONS IN MINOS EXPERIMENT

Until now we present a phenomenological framework for the off-diagonal MaVaN mechanism and show it changes the $\nu_\mu \to \nu_\mu$ atmospheric neutrino oscillation pattern in the SK experiment. However, the SK detector is not the only one sensitive to the neutrino oscillations in the $\nu_\mu \to \nu_\mu$ sector, and we can use the MINOS data [24] to constrain the nondiagonal MaVaN parameter. We show in Fig. 4 the comparison between the standard neutrino oscillation and the MaVaN probability for the setup of the MINOS experiment (using the $L = L_{MINOS}$ and the density $\rho_{crust} = 3.59$ g/cm^3). The oscillations parameters are fixed as $\Delta m^2_{32} = 2.5 \times 10^{-3}$ eV^2 and maximal mixing $\sin^2\theta_{23} = 1/2$. When we increase the MaVaN parameter we have for maximal mixing that the MaVaN amplitude get suppressed $\sin^2 2\theta_{\mathrm{MaVaN}} \to 0$, as you can see that the minimum, in Fig. 4, is less deep for higher values of the nondiagonal MaVaN parameter α_{32}. Since the oscillation phase, $\Delta m^2_{\mathrm{MaVaN}}$, is bigger for higher values of α_{32}, it implies that the minimum should be for higher values of energy. We also show for comparison in Fig. 4 the ratio of the experimental number of events over the theoretical prediction without oscillation as data points to emphasize that when we increase the value of the nondiagonal MaVaN parameter, we get further away from the experimental data.

So far we have shown examples of MaVaN effects for maximal vacuum mixing, $\sin^2\theta_{23} = 1/2$, e.g., in Figs. 1, 2, 3, and 4. A subtle effect can happen for the constant medium density case for larger values of the MaVaN parameter, α_{32}, in which case we have the MaVaN amplitude $\sin^2 2\theta_{\mathrm{MaVaN}} \to \cos^2 2\theta_{23}$, as mentioned in Sec. II. For small vacuum mixing angles θ_{23}, this implies that the amplitude is enlarged compared to without MaVaN, and for larger vacuum mixing angles θ_{23}, the situation is the opposite, and you have suppression of oscillation. To give an example we display in Fig. 5, the vacuum mixing angle $\sin^2 2\theta_{23}$ as a function of MaVaN parameter α_{32}, which gives a fixed value of MaVaN amplitude $\sin^2 2\theta_{\mathrm{MaVaN}} = 0.94$ [in another words the inverse function of Eq. (11)]. We can see that it has two solutions: one, the black curve, with small vacuum mixing angle $\sin^2 2\theta_{23}$, and the other given by the dashed red curve with large vacuum mixing angle.

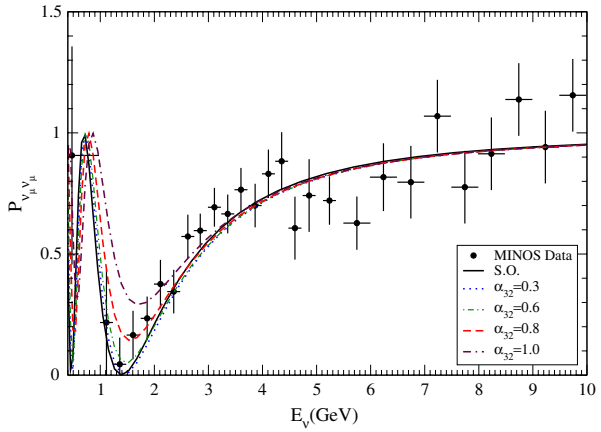

FIG. 4 (color online). Comparison between neutrino oscillations without (S.O.), solid line, and with MaVaN's, doted and dashed lines. The values of α_{32} are indicated in the figure. Also we assume $\sin^2\theta_{23} = 1/2$ and $\Delta m^2_{32} = 2.5 \times 10^{-3}$ eV^2. Points refer to MINOS data from [25].

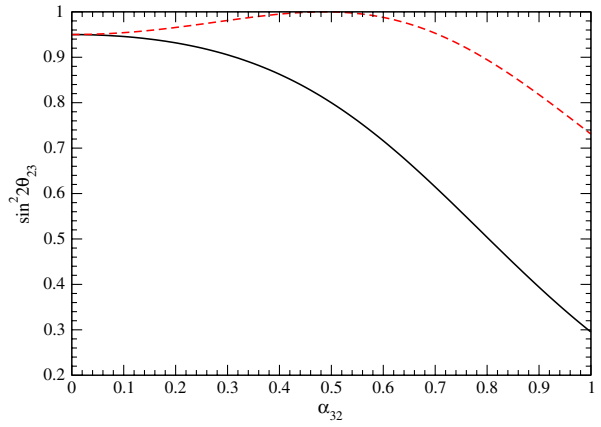

FIG. 5 (color online). The values of the vacuum mixing angle and α_{32} parameter that can made a fixed value for the MaVan amplitude $\sin^2 2\theta_{\mathrm{MaVaN}} = 0.94$.

This implies that we can have a small mixing angle and large α_{23} parameter or a large mixing angle and small parameter α_{23}, and both give an effective large MaVaN amplitude. For $\alpha_{23} \to \infty$, both curves coincide and we have full suppression of oscillation amplitude. We will see the consequences of this subtle effect later in our analysis in Sec. V.

V. ANALYSIS OF MINOS AND SUPER-KAMIOKANDE EXPERIMENT

Here we give the details of data analysis. First we begin with the analysis of the MINOS experiment and later the Super-Kamiokande analysis for the standard vacuum oscillation scenario and for the MaVaN scenario.

The MINOS experiment made a likelihood analysis of their data for neutrinos and antineutrinos for standard neutrino oscillation and produced a table with the values of $\sin^2 2\theta_{23}$, Δm^2_{32}, $\Delta \log L$, where $\Delta \log L = \log L/L_0$, where L is the likelihood value and L_0 is the likelihood for the best fit. This table is publicly available in Ref. [36]. We can translate the likelihood language into χ^2 language using $\Delta\chi^2 \equiv \chi^2 - \chi^2_{\mathrm{min}} = 2\Delta \log L$. For the MaVaN analysis, we can use the property that the MaVaN probability have the same functional form of standard oscillation, as discussed in Sec. IV, any function of probability also should have similar behavior. Therefore the $\chi^2_{\mathrm{S.O.MINOS\ analitic}}(\sin^2 2\theta_{23}, \Delta m^2_{32})$ function given in Ref. [36] as a function of $\sin^2 2\theta_{23}$ and Δm^2_{32}, should be equal to MaVaN $\chi^2_{\mathrm{MaVaN.MINOS\ analitic}}(\sin^2 2\theta_{\mathrm{MaVaN}}, \Delta m^2_{\mathrm{MaVaN}})$ as a function of the $\sin^2 2\theta_{\mathrm{MaVaN}}$ and $\Delta m^2_{\mathrm{MaVaN}}$ parameters. Numerically we have

$$\chi^2_{\mathrm{MaVaN.MINOS\ analitic}}(\sin^2 2\theta_{\mathrm{MaVaN}}, \Delta m^2_{\mathrm{MaVaN}}) = \chi^2_{\mathrm{S.O.MINOS\ analitic}}(\sin^2 2\theta_{23}, \Delta m^2_{32}), \quad (16)$$

where for the MINOS experiment we can use the expression for the MaVaN amplitude $\sin^2 2\theta_{\mathrm{MaVaN}}$ and mass difference $\Delta m^2_{\mathrm{MaVaN}}$, respectively, Eqs. (11) and (10) that give the MaVaN parameters as functions of the vacuum oscillation parameters $\sin^2 2\theta_{23}$ and Δm^2_{32}. We use this procedure to get the allowed region for MINOS only, for the standard oscillation scenario and for the MaVaN case. The results are shown in Fig. 6, where the dotted blue curve corresponds to the standard neutrino oscillations region of 90% C.L. As we plot the allowed region in the standard scenario as a function of $\sin^2\theta_{23}$ (and not a function of $\sin^2 2\theta_{23}$), the two degenerated minimums (denoted by "up" triangles) do appear. When we include MaVaN and minimize with respect to α_{32}, we get the allowed region given by the red dashed curve, which has the best fit

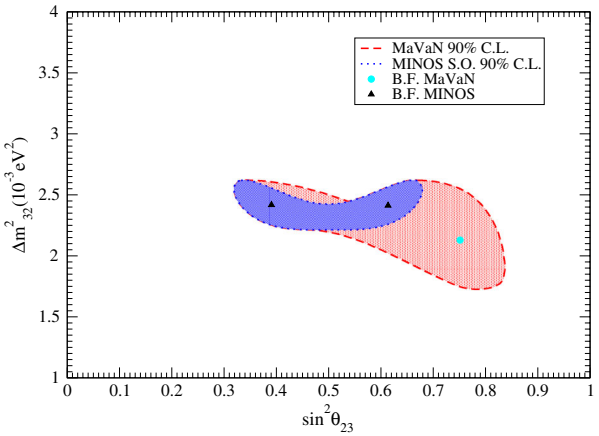

FIG. 6 (color online). Comparison of allowed region at 90% C.L. for oscillation parameters $(\Delta m^2_{32}, \sin^2\theta_{23})$ without (S.O), dotted blue line, and with MaVaN, dashed red line for the MINOS analysis.

for nonzero α_{32}, and for vacuum mixing angles smaller then maximal $\sin^2\theta_{23} = 0.8$ and mass differences $\Delta m^2 = 2.2 \times 10^{-3}$ eV^2. In the MaVaN allowed region, the mixing parameters can have larger values of $\sin^2\theta_{23}$ and smaller values of Δm^2_{32} that are not allowed in standard oscillation scenario. Smaller values of $\Delta m^2_{32} \sim 2 \times 10^{-3}$ eV^2 are not allowed in the standard scenario due it implies smaller oscillation effect that is in contradiction with the MINOS data, but in the MaVaN mechanism, the effective mass difference $\Delta m^2_{\mathrm{MaVaN}}$ can be larger then the vacuum oscillation mass difference compensating for the smaller value of Δm^2_{32}. Also the value of $\sin^2\theta_{23} \sim 0.8$ in the MaVaN solution, if we are working in the standard scenario, implies a smaller oscillation amplitude that also is not compatible with MINOS data. Also, we can allow values $\sin^2\theta_{23}$ far for maximal for nonzero α_{32}.

Now we will work with the analysis of SK data, where we will use the muon and electron data for sub-GeV and multi-GeV samples. The sample of atmospheric neutrino data is specially interesting for the MaVaN oscillation effect because it is composed by events produced by neutrinos traveling in vacuum and in matter from the use the muon and electron data for sub-GeV and multi-GeV sample as discussed in Sec. III.

To settle the basics of our analysis we should be aware that the predicted atmospheric neutrino flux has an uncertainty of 30% in the normalization and also a stronger correlation between the fluxes, with the relative error between the muon and electron flux is around 5% [31]. As said before, due to this normalization error we will test the shape of muon and electron distribution and not the absolute number of events. We made the following way, we are going to analyze the shape of atmospheric neutrino data and not include the comparison of the absolute value of data. To do this we will change our theoretical prediction of oscillation $N^{\gamma}_{\mathrm{theo}} \to (N^{\mathrm{renor}}_{\mathrm{theo}})^{\gamma} \equiv N_{\mathrm{theo}}\beta_{\gamma}$, where β_{γ} is the normalization parameter with a error of $\sigma_{\beta_{\gamma}} = 30\%$, with $\gamma = e, \mu$ for each flavor. Also we should use a correlation between the electron and muon number of events due to the correlation of the neutrino fluxes. We made two analyses:

(1) For the standard oscillation scenario to test our ability to reproduce the results of the SK analysis for the oscillation parameters Δm^2_{32} and $\sin^2(\theta_{23})$, we reproduce the main characteristics of $\Delta m^2_{32} \sim 3 \times 10^{-3}$ eV^2 and near maximal mixing
(2) The MaVaN scenario for nondiagonal parameter α_{23}, with $\alpha_{23} \neq 0$,

where our goal is reproduce the angular distribution predicted by SK experiment using our computation made independently of the SK experiment and from this to do a reliable analysis of MaVaN phenomena. Our choice of the χ^2 function is

$$\chi^2_{\mathrm{SK}}(\Delta m^2_{32}, \sin^2(\theta_{23}), \alpha_{32}) = \sum_{ij} (N^{\mathrm{data}} - \beta N^{\mathrm{theo}})_i (\sigma^2)^{-1}_{ij} \times (N^{\mathrm{data}} - \beta N^{\mathrm{theo}})_j + \frac{(\beta-1)^2}{\sigma^2_{\beta}}, \quad (17)$$

where N^{data}_i is the number of events in the bin i measured by SK, N^{teo}_i is our prediction for the number of events for the bin i that depend on the oscillation model used, the nondiagonal matrix $(\sigma^2)^{-1}_{ij}$ such that diagonal entries have error of 30% as said before, and the nondiagonal entries fixed by the correlation between the muon and electron flux [32]. The sum is over 40 bins, $40 = 10 \times 2 \times 2$, counting two flavors and two samples: sub-GeV or multi-GeV bins. We add the second term in Eq. (17) to introduce a penalty factor when β assume values too far from 1 with respect to the error in normalization, $\sigma_{\beta} = 0.3$.

The MINOS experiment tests the MaVaN scenario for a constant density that implies that the MaVaN parameters are fixed, and combining with SK experiment that test the MaVaN for variable density made specially adequate the main hypothesis of MaVaN idea, to have a mass difference and the mixing amplitude that depends on the local density. To achieve this we combine the two analyses from the MINOS experiment and the SK experiment, and we use the χ^2 test for both experiments,

$$\chi^2_{\mathrm{TOT}}(\sin^2\theta_{23}, \Delta m^2_{32}, \alpha_{32}) = \chi^2_{\mathrm{SK}} + \chi^2_{\mathrm{MINOS}}. \quad (18)$$

With this χ^2 with three oscillation parameters, we first analyze the standard oscillation scenario and second the MaVaN scenario for this combined analysis of MINOS and SK. We show the best-fit values for both scenarios in Table I. From this information we can see that there is a milder improvement of the MaVaN solution over the standard neutrino oscillation for the combining fit. For the MaVaN analysis of the combination of MINOS and SK, we have found that the best fit is for a nonzero value of MaVaN parameter $(\alpha_{32})_{\mathrm{B.F.}} = 0.28$ and the mixing parameters $(\Delta m^2_{32})_{\mathrm{B.F.}} = 2.45 \times 10^{-3}$ eV^2 and mixing angle $(\sin^2\theta_{23})_{\mathrm{B.F.}} = 0.46$ and the best-fit parameters for standard oscillation are very similar $(\Delta m^2_{32})_{\mathrm{B.F.}} = 2.42 \times 10^{-3}$ eV^2 and $(\sin^2\theta_{23})_{\mathrm{B.F.}} = 0.46(0.54)$ (see Table I). We show in the central panel of Fig. 7 the allowed region of Δm^2_{32} and

TABLE I. Summary of our χ^2 analysis for combined data from Super-Kamiokande and MINOS experiment. The first line corresponds to pure standard neutrino oscillations(S.O.) and the second line corresponds to the MaVaN scenario. In each case are show the best fit (B.F.) values of the parameters.

Model	$(\Delta m^2_{32}$ eV$^2)_{\mathrm{B.F.}}$	$(\sin^2\theta_{23})_{\mathrm{B.F.}}$	$(\alpha_{32})_{\mathrm{B.F.}}$	$\Delta\chi^2_{\mathrm{B.F.}}$
S. O.	2.42×10^{-3}	0.46 (0.54)	0.0	1.8
MaVaN	2.45×10^{-3}	0.46	0.28	0.0

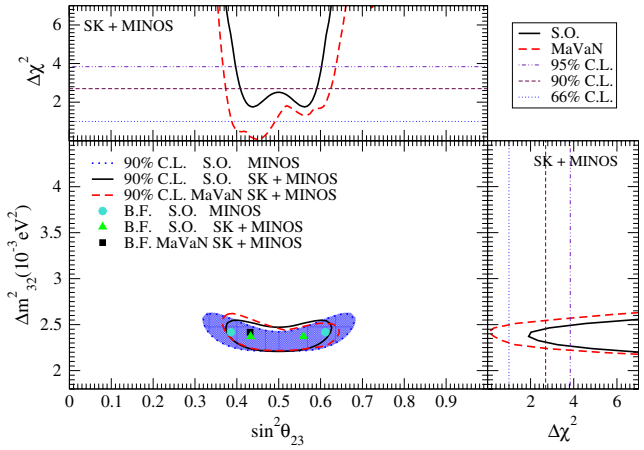

FIG. 7 (color online). In the center panel we show our result of combined analysis of MINOS and SK experiments for the allowed region of standard oscillation parameters $(\Delta m^2_{32}, \sin^2\theta_{23})$ for the cases with (dashed red curve) and without MaVaN effect (solid black line) compared with the result from MINOS Collaboration (dotted blue curve). We also show the values of best-fit points, respectively, in each analysis.

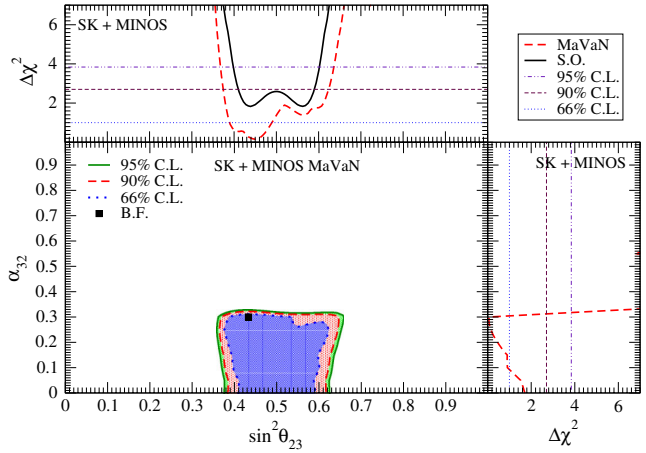

FIG. 8 (color online). In the center panel we show our result of combined analysis of MINOS and SK experiments for the allowed region of parameters $(\sin^2\theta_{23}, \alpha_{32})$ for 66% (dotted-dashed blue line), 90% (dashed red line), and 95% (solid green line) C.L. Black square is the best-fit point. The auxiliary upper plot is the same of Fig. 7. The left auxiliary plot refers to $\Delta\chi^2$ as function of α_{32} and minimized with respect to the other mixing parameters ($\sin^2\theta_{23}$ and Δm^2_{32}).

$\sin^2\theta_{23}$ parameters for the standard oscillation scenario (S.O.) and for the MaVaN scenario for the following cases:

(1) First for analysis of the standard oscillations (S.O.) in the MINOS experiment alone, shown by the dotted blue curve.
(2) Second, for the standard oscillations (S.O.) analysis for the combination of MINOS and SK experiments shown by the black curve. We can compare with the MINOS only result the improvement on the determination of range of $\sin^2\theta_{23}$ for the combination. The recent values from global fits for these parameters [37] are included in our 1σ allowed region for Δm^2_{32} and $\sin^2(2\theta_{23})$,
(3) Third, for the MaVaN scenario analysis for the combination of MINOS and SK experiments shown by dashed red curve, with

all plots shown in the 90% C.L. allowed region. Comparing the MaVaN allowed region for MINOS experiment only [shown in Fig. 6] and for the combination of MINOS and SK data [shown in central panel of Fig. 7], we see that combining the two experiments we constrain more the allowed region of parameters.

Another good tool to understand our solution is the plot of the projection of $\Delta\chi^2 \equiv \chi^2_{\rm TOT} - \chi^2_{\rm B.F.}$ function with respect to the one of three oscillation parameters, $\sin^2\theta_{23}$, Δm^2_{32}, and α_{32}. When we show the projection, e.g., for example $\Delta\chi^2 \times \Delta m^2_{32}$, we have minimized over the other parameters, $\sin^2\theta_{23}$ and α_{32}, and so on. We begin with the top panel of Fig. 7, where we show the plot of the projection of $\chi^2 \times \sin^2\theta_{23}$ for the standard oscillation (black curve) and MaVaN (dashed red curve) together with the 66%, 90%, and 95% C.L., respectively, $\Delta\chi^2 = 1.0$, 2.70, 3.84. We can see that the combination of MINOS and SK suppresses the high values of $\sin^2\theta_{23} > 0.7$ that are present in the MINOS-only analysis, where they appear only at high C.L. (not shown) when we have $\Delta\chi^2 > 7$. These high values are only possible in MINOS analysis for $\alpha_{32} > 0.7$; however, this large value will induce stronger changes in oscillation probabilities for the SK experiment due to larger density than the neutrino feels when crossing the Earth. Typically we have $\rho_{\rm SK} > (2-3)\rho_{\rm MINOS}$. We notice in Fig. 1 that for $\alpha_{32} > 0.7$, we expect to see a stronger suppression of the muon neutrino oscillation that will conflict the SK data. In the right panel of Fig. 7 we show the plot of the projection of $\chi^2 \times \Delta m^2_{32}$ for both the standard oscillation and the MaVaN scenario, respectively, by black and dashed red curve. We can see a slight increase in the allowed region for Δm^2_{32} when we have a nonzero MaVaN parameter. We show in the central panel of Fig. 8 the allowed region of parameters $(\sin^2\theta_{23}, \alpha_{23})$ and minimized with respect to Δm^2_{32} at 66%, 90%, and 95% C.L. You can see from this plot that there is a correlation between the $\sin^2\theta_{23}$ and α_{23} for the range of values allowed. For the highest α_{32} value, we have the widest range for $\sin^2\theta_{23}$. This is left over from the behavior discussed in Sec. IV, where we have a smaller vacuum mixing amplitude for higher α_{32} or a large vacuum mixing amplitude for smaller α_{32}. In the right panel we show the plot of the projection of $\chi^2 \times \alpha_{23}$, where we can see the standard oscillation scenario (when $\alpha_{32} = 0$) is compatible at $\Delta\chi^2 = 1.8$, and the more interesting information from this plot is that there is no allowed region for $\alpha_{32} > 0.32$ at 90% C.L. The solutions for higher $\alpha_{32} > 0.5$ presented in the MINOS analysis only appear now for the combined

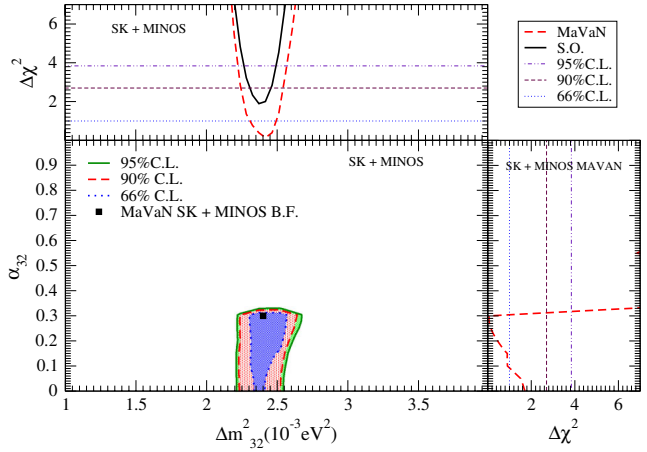

FIG. 9 (color online). In the center panel we show our result of combined analysis of MINOS and SK experiments for the allowed region of parameters $(\Delta m^2_{23}, \alpha_{32})$ for 66% (dotted-dashed blue line), 90% (dashed red line), and 95% (solid green line) C.L. Black square is the best-fit point. The auxiliary upper (right) plot refers to $\Delta\chi^2$ as function of $\Delta m^2_{32}(\alpha_{32})$ and minimized with respect to other parameters.

analysis at $> 99\%$ C.L. for the same reasons discussed in the previous paragraph.

Finally, for completeness, in the central panel of Fig. 9 we show the allowed region of parameters as a function of Δm^2_{23}, α_{32}. In this central panel, we can see that the correlation between the values of Δm^2_{23} and α_{32} are much milder than between the $\sin^2\theta_{23}$, α_{32} as shown in Fig. 8. The reason for this is that the change in $\Delta m^2_{\mathrm{MaVaN}}$ due to α_{32} is not so much stronger compared with the change in $\sin^2\theta_{\mathrm{MaVaN}}$.

VI. CONCLUSION

In this paper we test the possibility of neutrinos have their mass dependent on the medium density. The so-called MaVaN model includes this new feature through a new neutrino interaction mediated by a scalar field. We investigate the consequences of such a model in the phenomenology of atmospheric neutrino data from the Super-Kamiokande experiment and for the MINOS experiment, using for the first time to test the existence of the nondiagonal MaVaN parameter.

Using the fact that the MaVaN for the constant matter density, as is the case for the MINOS experiment, have the same functional form as in the standard oscillation scenario, we use the MINOS analysis for the standard neutrino oscillation and we extend for the MaVaN scenario. In this analysis, larger values of the nondiagonal MaVaN parameter, $\alpha_{32} > 0.7$, are allowed and we have significant changes in the allowed region for oscillation parameters, Δm^2_{32} and $\sin^2(\theta_{23})$.

We compute by ourselves the event rate for the Super-Kamiokande experiment, involving the correct description of the sub-GeV and multi-GeV neutrino energy samples, and we also use the analysis of the MINOS experiment to make a combined fit of these two experiments. In the MINOS experiment the neutrino crosses only a small chord of the Earth and then the neutrino feels a constant matter density; for the other side, the Super-Kamiokande have neutrinos coming from different directions, and therefore they feel different medium densities. Then by combining the two data, we can test the essence of the MaVaN hypothesis, the mass dependence on the medium density. We have found that the best-fit values for $\Delta m^2_{32} = 2.45 \times 10^{-3}$ eV^2, $\sin^2(\theta_{23}) = 0.42$, and the MaVaN parameter $\alpha_{32} = 0.28$ and the best-fit values for the standard oscillation give similar values [see Table I].

The allowed region for the oscillation parameters, Δm^2_{32} and $\sin^2(\theta_{23})$, is shown in Fig. 7, illustrating that the allowed region is very stable with the addition of the MaVaN scenario. Although the best fit is for the nonzero MaVaN parameter, we have all values of the MaVaN parameter $\alpha_{32} > 0.31$ ruled out at 90% C.L., which allows us to conclude that the nondiagonal MaVaN coupling should give a smaller contribution to neutrino oscillation.

ACKNOWLEDGMENTS

The work of D. R. G. is supported by CAPES and CNPQ. O. L. G. P. thanks the ICTP and the financial support from Grant No. 2012/16389-1, São Paulo Research Foundation (FAPESP).

[1] J. Tauber *et al.* (Planck Collaboration), Astron. Astrophys., doi: 10.1051/0004-6361/201321529 (2013).
[2] A. Jae *et al.* (Planck Collaboration), Astron. Astrophys., doi: 10.1051/0004-6361/201321546 (2013).
[3] M. Tegmark *et al.* (SDSS Collaboration), Phys. Rev. D **74**, 123507 (2006).
[4] A. G. Riess *et al.* (Supernova Search Team Collaboration), Astron. J. **116**, 1009 (1998).
[5] S. Perlmutter *et al.* (Supernova Cosmology Project Collaboration), Astrophys. J. **517**, 565 (1999).
[6] P. Astier *et al.* (SNLS Collaboration), Astron. Astrophys. **447**, 31 (2006).

[7] A. Einstein, Sitzungsber. Preuss. Akad. Wiss. Berlin (Math. Phys.) **1917**, 142 (1917).
[8] S. Weinberg, Rev. Mod. Phys. **61**, 1 (1989).
[9] A. D. Dolgov, in *Proceedings of 18th Les Rencontres de Physique de la Vallee d'Aoste*, Frascati Physics Series, edited by M. Greco (INFN, Frascati, Rome, 2004), Vol. 34.
[10] R. Fardon, A. E. Nelson, and N. Weiner, J. Cosmol. Astropart. Phys. 10 (2004) 005.
[11] D. B. Kaplan, A. E. Nelson, and N. Weiner, Phys. Rev. Lett. **93**, 091801 (2004).
[12] P. Gu, X. Wang, and X. Zhang, Phys. Rev. D **68**, 087301 (2003).
[13] X.-J. Bi, P.-h. Gu, X.-l. Wang, and X.-m. Zhang, Phys. Rev. D **69**, 113007 (2004).
[14] N. Afshordi, M. Zaldarriaga, and K. Kohri, Phys. Rev. D **72**, 065024 (2005).
[15] M. Honda, R. Takahashi, and M. Tanimoto, J. High Energy Phys. 01 (2006) 042.
[16] V. Barger, P. Huber, and D. Marfatia, Phys. Rev. Lett. **95**, 211802 (2005).
[17] M. Cirelli, M. C. Gonzalez-Garcia, and C. Pena-Garay, Nucl. Phys. **B719**, 219 (2005).
[18] M. C. Gonzalez-Garcia, P. C. de Holanda, and R. Zukanovich Funchal, Phys. Rev. D **73**, 033008 (2006).
[19] P. C. de Holanda, J. Cosmol. Astropart. Phys. 07 (2009) 024.
[20] F. Rossi-Torres, M. M. Guzzo, P. C. de Holanda, and O. L. G. Peres, Phys. Rev. D **84**, 053010 (2011).
[21] M. F. Carneiro and P. C. de Holanda, Adv. High Energy Phys. **2013**, 293425 (2013).
[22] K. K. Shiraishi, Ph.D. thesis, University of Washington, 2006; http://www-sk.icrr.u-tokyo.ac.jp/doc/sk/pub/.
[23] K. Abe *et al.* (Super-Kamiokande Collaboration), Phys. Rev. D **77**, 052001 (2008).
[24] P. Adamson *et al.* (MINOS Collaboration), Phys. Rev. Lett. **110**, 251801 (2013).
[25] P. Adamson *et al.* (MINOS Collaboration), Phys. Rev. Lett. **106**, 181801 (2011).
[26] In the MaVaN mechanism, neutrino and antineutrinos have the same oscillation probability.
[27] D. R. Gratieri, Ph.D. thesis, State University at Campinas (UNICAMP), 2012; http://webbif.ifi.unicamp.br/tesesOnline/teses/IF1564.pdf.
[28] A. D. Dziewonski and D. L. Anderson, Phys. Earth Planet. Inter. **25**, 297 (1981).
[29] For a good reference on kinematical constraints, see [30].
[30] V. I. Goldanski, and I. L. Rosenthal, *Kinematics of Nuclear Reactions* (Oxford University Press, New York, 1961).
[31] M. Honda, T. Kajita, K. Kasahara, S. Midorikawa, and T. Sanuki, Phys. Rev. D **75**, 043006 (2007).
[32] M. C. Gonzalez-Garcia, H. Nunokawa, O. L. G. Peres, T. Stanev, and J. W. F. Valle, Phys. Rev. D **58**, 033004 (1998).
[33] A. Strumia and F. Vissani, Phys. Lett. B **564**, 42 (2003).
[34] E. A. Paschos and J. Y. Yu, Phys. Rev. D **65**, 033002 (2002).
[35] J. Hosaka *et al.* (Super-Kamiokande Collaboration), Phys. Rev. D **74**, 032002 (2006).
[36] The χ^2_{MINOS} is avaliable in http://www-numi.fnal.gov/PublicInfo/forscientists.html.
[37] M. C. Gonzalez-Garcia, M. Maltoni, J. Salvado, and T. Schwetz, J. High Energy Phys. 12 (2012) 123.